

# Secondary Structure Formation in Hybrid Synthetic/Peptide Polymers: Insights from Molecular Dynamics Simulations

Thomas Kunze, Christian Dreßler, and Daniel Sebastiani\*

Proteins and peptides exhibit an immense variety of structures, which are generally classified according to simple structural motifs (mainly  $\alpha$  helices and  $\beta$  sheets). Considerable efforts have been invested in understanding the relationship between chemical structure (primary structure) of peptides and their spatial motifs (secondary structure). However, little is known about the possibility to interfere intentionally in these structural driving forces, for example, by inserting (short) artificial polymer chains in the peptide backbone. Structure formation on such hybrid synthetic/biochemical polymers is still an emerging field of research. Here, molecular dynamics simulations are used to illustrate the influence of inserted polyethylene segments on the secondary structure of several peptide homopolymers. A loss of structure of  $\approx 50\%$  when the peptide chain length drops to ten amino acids and a practically complete absence for even shorter peptide segments.

## 1. Introduction

### 1.1. Introduction to Project A09 of the SFB/TRR 102 “Polymers under Multiple Constraints”

This work was part of the third funding phase (2019–2023) of project A9 of the Collaborative Research Centre SFB/TRR 102, funded by the German Science Foundation (DFG). In the first two periods (2012–2015 and 2015–2019, respectively), the research focus was initially put on ions and small functional segments of biomolecules, such as chromophores, and their interaction with solvent molecules. Specifically, the first funding period (2011–2015) resulted in a series of investigations of aqueous solutions

of simple and complex ions,<sup>[1–3]</sup> in combination with their spectroscopic fingerprints.<sup>[1,4]</sup> Nevertheless, specific features of individual protein systems were already simulated as well.

In the second funding period (2015–2019), the focus shifted to the investigation of conformational variations of small amyloidogenic proteins due to specific mutations which modify the equilibrium of intra-protein interactions and protein–solvent interactions.<sup>[5]</sup> In parallel, the interactions of salt ions with solvating water molecules and the interaction equilibrium between a typical protein salt bridge and the solvating water molecules complemented this picture.<sup>[6–8]</sup> Special attention was again paid to the importance of spectroscopic signatures, both regarding infrared<sup>[6,7]</sup> and NMR

spectroscopy.<sup>[5,9]</sup> Finally, during the third funding period (2019–2023), the project has evolved toward two distinct directions: general polymer structure formation and functional hybrid organic/inorganic copolymers in the context of energy storage/conversion.


The first direction is the continuation of the collaborations on polymer structure formation, which comprises the analysis of secondary structure perturbation of peptide chains via flexible polyethylene segments (research part of this article), the understanding of induced helicity in an achiral polymer via a single chiral monomer within the polymer (collaboration with project A03), and the development of reverse coarse-graining scheme for benchmarking the sampling quality of a coarse-grained simulation run of systems such as polyglutamine (collaboration with project A07), as well as the interplay between polymer structure (here: cellulose) and the solubility in different kinds of solvents.<sup>[10]</sup>

On the other hand, a second direction has emerged from the consideration of novel types of polymers, specifically hybrid organic/inorganic copolymers. On the example of crosslinked organic/sulfur compounds, we have started an investigation about local packing effects and lithium diffusion/lithiation reactions in the presence of lithium ions.<sup>[11]</sup> Beforehand, a preliminary study dealt with the understanding of lithium diffusion in amorphous thiophene.<sup>[12]</sup> This research line is presently intensified and will give rise to novel projects in the context of renewable energies.

Concluding this survey of topic of this project A09, we want to spotlight a methodological project line that has emerged from the successful collaboration with project A07 (W. Paul). In our joint study of polyglutamine and its conformational distribution in aqueous solution,<sup>[13]</sup> we have established an inverse coarse

T. Kunze, D. Sebastiani  
Martin-Luther University Halle-Wittenberg  
Institute for Physical Chemistry  
Von-Danckelmann-Platz 4, 06120 Halle/Saale, Germany  
E-mail: daniel.sebastiani@chemie.uni-halle.de

C. Dreßler  
Institute of Physics  
Ilmenau University of Technology  
Weimarer Straße 32, 98684 Ilmenau, Germany

 The ORCID identification number(s) for the author(s) of this article can be found under <https://doi.org/10.1002/mats.202200070>

© 2023 The Authors. Macromolecular Theory and Simulations published by Wiley-VCH GmbH. This is an open access article under the terms of the Creative Commons Attribution License, which permits use, distribution and reproduction in any medium, provided the original work is properly cited.

DOI: 10.1002/mats.202200070

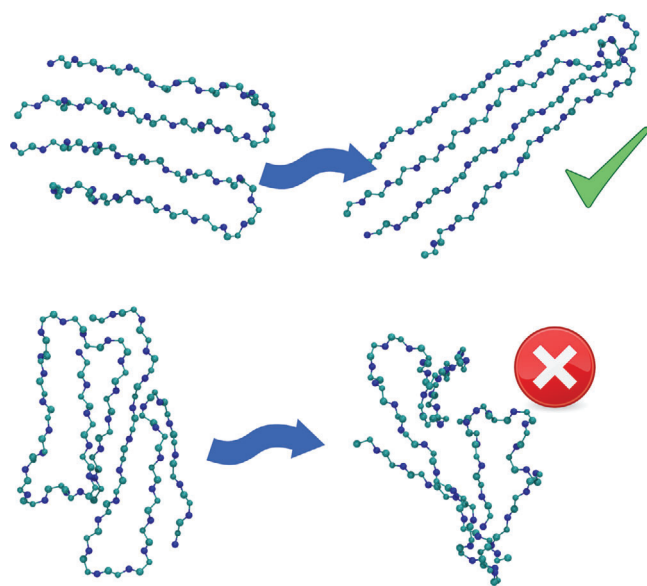


**Figure 1.** Illustration of the result of the inverse coarse-graining procedure from the PRIME20 peptide model to atomistic resolution, on the example of a (Gln)<sub>22</sub> dimer. Two example conformations are shown: on the left, the atomistic structure directly reconstructed from the PRIME20 conformation; on the right, the corresponding structure after 10 ns of equilibration via atomistic molecular dynamics simulations (in aqueous solution). The upper conformation remains stable (apart from a global rotation), while the lower structure changes significantly, marking an enthalpically unfavorable conformation of the PRIME20 sampling.

graining protocol for the PRIME20 coarse grained protein model.<sup>[14]</sup> We have designed a computational scheme to re-establish a tentative atomistic structure of the glutamine oligopeptide after conformational sampling with at the coarse-grained level using the PRIME20 model. The tentative structures are then equilibrated for a short period of 10 ns using all-atom molecular dynamics simulations, and the degree of structural deviation from the tentative conformation is measured. Using this scheme, we are able to validate the phase space sampling quality of the PRIME20 interaction scheme.

An illustration of the application potential of our scheme is shown in **Figure 1** on the example of a glutamine-22 dimer. Two structures (upper left and lower left) have been obtained from the PRIME20 conformational sampling scheme, using the inverse coarse-graining algorithm. Subsequently, molecular dynamics simulation have been performed for 10 ns in aqueous solution, yielding the atomistic conformations shown in the upper right and lower right parts of **Figure 1**. While the upper conformation has only rotated in space but otherwise remained unchanged, the lower structure has changed significantly during the equilibration run. Such a situation indicates that the particular conformation as obtained from the PRIME20 conformational sampling does not represent a local minimum of the potential energy landscape and should thus be discarded. Preliminary results indicate that the majority of the conformations generated by the PRIME20 sampling approach are “good” structures which represent stable conformations also within the atomistic equilibration run. Particular focus will be put on the correlation between the

energies computed at the coarse grained level and those obtained from the atomistic molecular dynamics simulation.

## 1.2. Introduction to this Research

Proteins have a significant role in our body, ranging from metabolism, defense mechanisms to structural functions in skin and bones amongst many others. With a wide range of functions there is also the possibility of multiple malfunctions, noticeable by the huge amount of diseases caused by misfolded proteins. Notoriously Alzheimer's,<sup>[15]</sup> Huntington's,<sup>[16]</sup> and Parkinson's<sup>[17]</sup> are some of the most commonly known neurodegenerative diseases attributed to the toxicity after a structural change and following aggregation.<sup>[18]</sup> This transition can occur for multiple reasons, including temperature, pH-value, additives, and solvent.<sup>[19–21]</sup>

A therapeutic approach curing these diseases consists of molecules similar to the aggregating proteins but with the ability to destabilize the aggregating conformation.<sup>[22]</sup> This was already tried with so called  $\beta$ -sheet breaker inhibiting and dissolving amyloid- $\beta$  structures, which are the cause for Alzheimer's disease.<sup>[18,23]</sup> Since there has not been any major success for this complex problem yet, new models and approaches are discussed.<sup>[24,25]</sup> Such conformation inducing compounds can often be found as peptides, especially as copolymers to obtain a specific drug delivery system.<sup>[26–29]</sup> The use of peptide containing hybrid copolymers,<sup>[30]</sup> not only enables a possibly nontoxic drug delivery system, it can also influence the secondary structure to well-defined physical characteristics.<sup>[31–35]</sup>

The synthetic preparation of hybrid polymers can be achieved by acyclic diene metathesis (ADMET) polymerization in hexafluoroisopropanol (HFIP) or trifluoroethanol (TFE), which takes already prepared oligopeptides, adding alkenes on both sides to polymerize multiple of these molecules by metathesis.<sup>[30,36,37]</sup> The base oligopeptides can be obtained by ring-opening polymerization (ROP), however full natural proteins were previously only available by the Merrifield's method, which can only produce small peptides at high costs.<sup>[38–40]</sup> By advancement in chemical protein synthesis powerful alternative synthesis methods are now available to produce large previously unobtainable proteins, however this approach deals with different difficulties such as solubility and purification among others.<sup>[41]</sup>

For industrial purposes, the research of hybrid polymers is focused on effectively enhancing or substituting widely used bulk polymers with biopolymers to increase biodegradability and environmentally friendly production.<sup>[42]</sup> This includes materials for packaging even in the food industry,<sup>[43]</sup> polymers which are able to form nanomaterials<sup>[44]</sup> used in water purification<sup>[45]</sup> or medical supply like implants.<sup>[46]</sup> Combining synthetic and biopolymers gives a whole new class of materials, that has the prospect to utilize the best properties of both. One of the main advantages of incorporating biological segments into hybrid polymers is the structural control, for example, given by the secondary structure of peptide segments.<sup>[47]</sup> This control includes regulated structure transitions caused by pH- or temperature-change among other things.<sup>[48]</sup> However, the application of hybrid peptide-copolymers is mostly limited to drug delivery applications as of now,<sup>[49]</sup> but

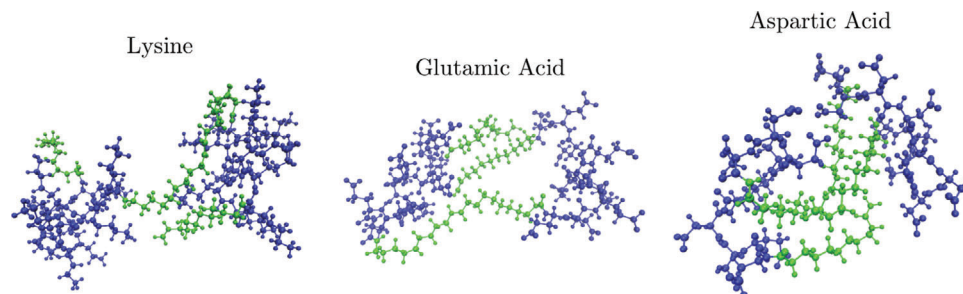


**Figure 2.** Snapshots of molecular structures of  $[PE-(AA)_{10}]_2$  molecules (left to right: Lys, Glu, Asp) during the molecular dynamics simulation. The explicit solvent molecules are not shown.

upon further research could also have an impact on functional surfaces or biomineralization.<sup>[50]</sup>

For structural analysis a set of different techniques is feasible, including circular dichroism (CD) as well as Fourier transformed infrared (FTIR) spectroscopy in solution and solid-state.<sup>[51–53]</sup>

In this work, the interplay of synthetic and peptide segments in hybrid polymers is investigated. We focus on the insertion of a specific type of synthetic polymer segment into a series of model peptides. We determine characteristic conformational motifs and their dependence on the chemistry of the hybrid molecule, specifically amino acid (AA) type and length. A particular focus lies on the attempt to identify conformational patterns induced by the different geometric chain flexibility, but also the type of philicity of the polymer segments: while the PE chains are the textbook example of hydrophobic molecules, the charged peptide segments have a distinctly hydrophilic character.

An illustration of three hybrid polymers investigated is given in **Figure 2**.

Studies on the structure of homopeptides have been done for a long time, often by using circular dichroism spectroscopy. For lysine (Lys) oligomers the structure is random for short peptides and gets more helical content with increasing length and even more so at higher pH values.<sup>[54]</sup> Glutamic acid (Glu) peptides show similar behavior, transitioning from random to helical structure starting at  $n = 10$  and having a full helical structure after  $n = 50$ .<sup>[55]</sup>

With the insertion of a PE chain into the continuous homopeptide, stronger hydrophobic forces get introduced into the molecule. These new integrated forces are opposed to the peptide intra-molecular and solvent hydrogen bonds and will therefore result in conformations with reduced solvent accessible surface area compared to peptides with similar overall length. In **Figure 2** common established structures are visualized. The green PE chains show multiple possible positions in regard to peptides and other PE chains. While this qualitative trend is obvious, we presently have little quantitative understanding of how exactly the peptide conformation is influenced by the geometric flexibility and the hydrophobic forces due to the artificial PE chains. This is the primary aspect that is addressed in the following, using atomistic molecular dynamics simulations.

## 2. Experimental Section

The chemical structure of the small model hybrid systems are shown in **Figure 3**, with peptides connected by a PE chain similar

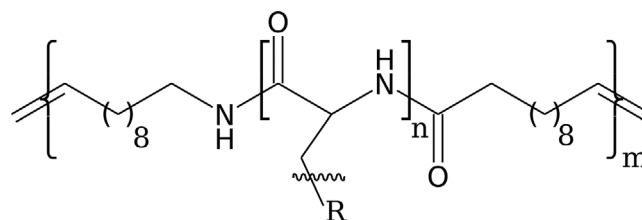


**Figure 3.** Structure of hybrid polymers composed of a homopeptide with amino acid (AA=Asp, Lys, Glu), which is connected to a short polyethylene chain. The double bond which connects two such hybrid monomers is maintained during synthesis.<sup>[30,36,37]</sup>

**Table 1.** Summary of computational parameters for all sets of hybrid polymers. While the temperature  $T_{\max}$  of the highest of  $N_{\text{repl}}$  replica differs for the systems, the temperature  $T_{\text{system}}$  for the calculation of the lowest replica, which is the one considered for analysis, remains the same. (AA=Asp, Lys, Glu).

Polymer type	$T_{\max}$ [K]	$N_{\text{repl}}$	$T_{\text{system}}$ [K]
$[PE-(AA)_{10}]_2$	500	16	300
$[PE-(AA)_3]_2$	700	16	300
$[PE-(AA)_3]_6$	600	16	300

to experimentally investigated hybrid polymers.<sup>[30,36,37]</sup> The peptides were varied in length and amino acid type (AA=Asp, Lys, Glu).

The hybrid polymers were simulated with classical molecular dynamics simulations using the enhanced sampling technique Hamiltonian replica exchange<sup>[56]</sup> with solute tempering 2 (REST2)<sup>[57,58]</sup> implemented by PLUMED<sup>[59]</sup> into GROMACS version 2019.1.<sup>[60,61]</sup> The CHARMM27<sup>[62,63]</sup> force field was used to calculate the hybrid polymer interactions and solvation effects of water were calculated with the TIP3P water model. Each type of hybrid molecule was put elongated into cubic box filled with water, ranging from 6 to 10 nm depending on the hybrid molecule's size. All amino acid sidechains were charged, therefore the whole system was neutralized afterward with chloride or sodium ions. Overall 16 replica per system were used starting at 300 K and ranging up to 500 to 700 K, again dependent on the system size to achieve average exchange probabilities ranging from 10% to 40%, summarized in **Table 1**. With a Lincs<sup>[64]</sup> fourth order linear constraint for covalent hydrogen bonds the time step was kept at 0.5 fs for technical reasons at early equilibration with replica

**Table 2.** Secondary structure analysis of all hybrid polymers and references. Shown is the integral of characteristic regions in the Ramachandran plot, which correspond to typical secondary structure motifs.

Hybrid polymer	$\alpha$ -helix	$\beta$ -sheet	Other
[PE-(Asp) <sub>3</sub> ] <sub>2</sub>	0.74	0.22	0.04
[PE-(Asp) <sub>3</sub> ] <sub>6</sub>	0.61	0.18	0.21
[PE-(Asp) <sub>10</sub> ] <sub>2</sub>	0.83	0.15	0.02
6× Asp <sub>3</sub>	0.55	0.32	0.13
2× Asp <sub>10</sub>	0.73	0.26	0.01
[PE-(Glu) <sub>3</sub> ] <sub>2</sub>	0.75	0.20	0.05
[PE-(Glu) <sub>3</sub> ] <sub>6</sub>	0.65	0.22	0.13
[PE-(Glu) <sub>10</sub> ] <sub>2</sub>	0.87	0.11	0.02
6× Glu <sub>3</sub>	0.49	0.38	0.13
2× Glu <sub>10</sub>	0.82	0.17	0.01
[PE-(Lys) <sub>3</sub> ] <sub>2</sub>	0.79	0.14	0.07
[PE-(Lys) <sub>3</sub> ] <sub>6</sub>	0.70	0.19	0.11
[PE-(Lys) <sub>10</sub> ] <sub>2</sub>	0.81	0.15	0.04
6× Lys <sub>3</sub>	0.50	0.35	0.15
2× Lys <sub>10</sub>	0.92	0.02	0.06

exchange attempt every 200 steps. The simulations were run for 60 ns and analyzed with built-in GROMACS tools for hydrogen bonding, radius of gyration ( $R_g$ ) and Ramachandran plots. All other analysis was performed by TRAVIS<sup>[66,67]</sup> and visualization was carried out by VMD.<sup>[65]</sup> Analysis started after 20 ns of initial calculation. The [PE-(Glu)<sub>3</sub>]<sub>6</sub> system was run for 90 ns, however no significant difference in any of the relevant conformational distributions was found. The reference calculation for the homopeptides used the same parameters, however without the replica exchange method. The termini of the peptide were capped by *N*-methyl (NME) and acetyl (ACE) to reduce the effect of the termini and as a result have a better reference.

### 3. Results

#### 3.1. Hybrid Polymer with Single Embedded PE Chain

Our focus lies on the formation of structural motifs at a more general level, specifically the characterization of hybrid polymers in terms of the spatial arrangement of the peptide and PE segments. With this goal in mind we have determined structural parameters, which we have found to be suitable to describe (and discriminate) the overall conformations of our hybrid polymers. For reference we analyzed the peptides without the PE-chains, shown as “6× AA<sub>3</sub>” and “2× AA<sub>10</sub>” in **Table 2**.

One of the main characteristics of peptide secondary structures is the formation of helical or hairpin structure (helices, sheet-like structures). Our starting point was therefore to analyze the degree of helicity, which the hybrid polymers are able to establish. To derive an approximate conformational statistics, we calculated the Ramachandran plots and quantified the secondary structure regions approximately. The Ramachandran plot itself is a representation of the backbone angles ( $\psi$ ,  $\phi$ ), thereby each secondary structure correlates to a specific region in the plot. Accumulating all points in these specific regions leads to a roughly

estimated distribution of secondary structures. The results in **Table 2** show similar behavior, observing roughly 75%  $\alpha$ - and 15%  $\beta$ -structures for all types of molecules. Some hybrids show more equal behavior, for example, [PE-(AA)<sub>10</sub>]<sub>2</sub> and [PE-(AA)<sub>3</sub>]<sub>2</sub>. Visual inspection however shows differences between the amino acids comparing the snapshots in **Figures 4** and **2**, which are not represented by the Ramachandran plot. Hence, it turns out this broadly used analysis does not give satisfactory structural classification for very short peptide segments. The underlying reason is that short peptides exhibit characteristic backbone angles without adopting the corresponding secondary structure motifs.

Another aspect of the structure formation for our hybrid systems is the behavior of the PE chains. Consequently, we calculated radial distribution functions (RDF) of the PE chains  $d(\text{PE-PE})$ . The polyethylene-polyethylene distance  $d(\text{PE-PE})$  is calculated as the distance between the central carbon atoms of the polyethylene chains. These central carbon atoms are marked in purple in the snapshot in **Figure 4** (top left). The number as well as the positions of the maxima of the RDFs differ for each amino acid AA = Asp, Glu, Lys in the hybrid polymer series [PE-(AA)<sub>10</sub>]<sub>2</sub>. In contrast, the RDFs of the small peptide-polyethylene hybrid molecules of the type [PE-(AA)<sub>3</sub>]<sub>2</sub> have similar shapes and only one distinct maximum. The RDFs of the hybrid-polymers of the type [PE-(AA)<sub>3</sub>]<sub>6</sub> show a rather similar behavior compared to the RDFs of the hybrid-polymer [PE-(AA)<sub>3</sub>]<sub>2</sub>. Based on the analysis of the RDFs, we can conclude that bigger peptides have greater PE-PE distances and are stronger affected by the type of the amino acid. In order to explain the origin of these observation, we have therefore switched to more complex geometric parameters in order to capture more detail of the genuine peptide structure via the intercalated PE chains. Specifically, we have found two particular distances that are able to describe and discriminate our hybrid polymers. The first parameter is the distance between centers of masses of a PE chain and a peptide segment  $d(\text{PE-AA})$  with AA=Asp, Glu, Lys. Note that each pair of PE chain/peptide segment is considered (not only the adjacent chain). The other parameter  $d(\text{PE-PE})$  is the distance between the center of mass of a given PE chain to the center of mass of another, not necessarily adjacent, PE chain.

With the two given parameters  $d(\text{PE-PE})$  and  $d(\text{PE-AA})$  the structure was analyzed by a combined distribution function<sup>[66,67]</sup>  $g(d(\text{PE-AA}), d(\text{PE-PE}))$ . This function represents the 2D probability distribution for the simultaneous occurrence of a given PE-AA distance and a given PE-PE distance.

A particular feature of this set of parameters is the explicit incorporation of molecular philicity: The combined distribution function of  $d(\text{PE-PE})$  and  $d(\text{PE-AA})$  allow the analysis of aggregation effects due to segments of same philicity (PE-PE) and opposite philicity (PE-AA). Notably, the distances between PE chains also give information about the secondary structure, since the PE segments are the linking parts between peptides. This way, a linear elongated peptide will yield larger PE-PE distances, while secondary structure features like helices or turns will result in nearby PE-PE distances.

The results of the radial distribution functions  $g(d(\text{PE-AA}), d(\text{PE-PE}))$  for the [PE-(AA)<sub>10</sub>]<sub>2</sub> systems are shown in **Figure 5**. The hybrid polymers exhibit distinctly different patterns for the three amino acids. Each type has an individual pattern of highly

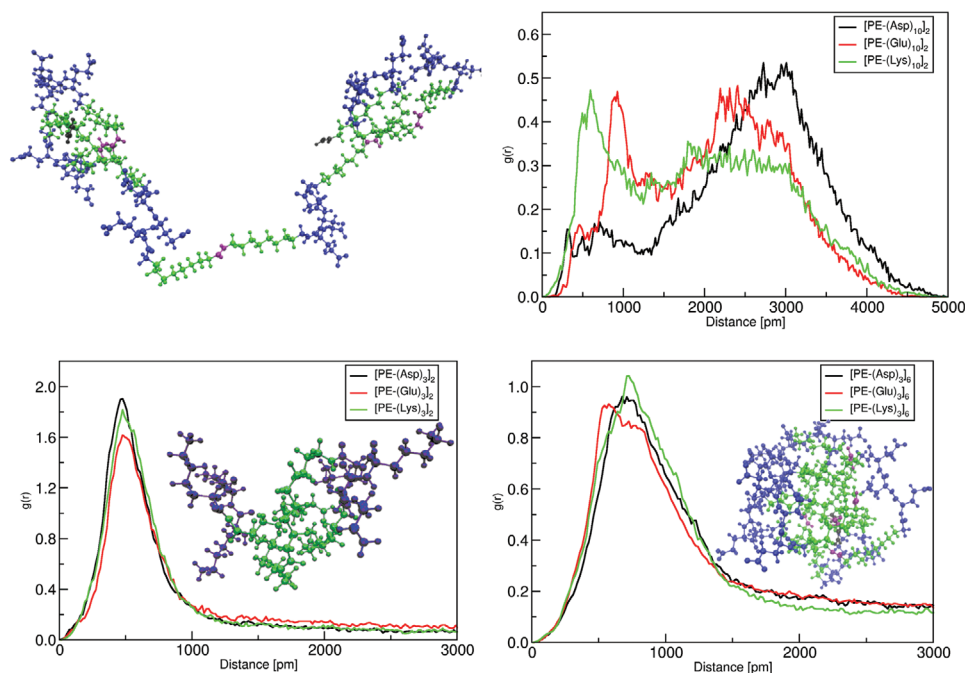


**Figure 4.** Radial distribution functions of the distances  $d(\text{PE-PE})$  between two polyethylene chains for the different hybrid polymers. Herein, the polyethylene–polyethylene distance  $d(\text{PE-PE})$  is calculated as the center of mass of the PE-chain. Note that the positions of the terminating polyethylen chains are also included into the calculation of the RDFs.

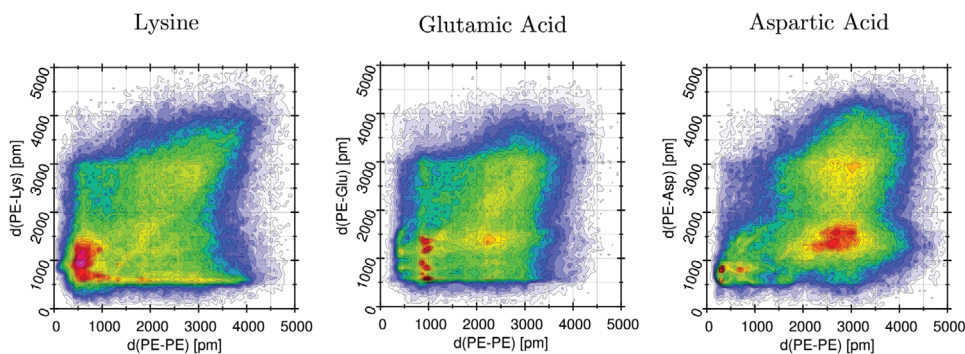


**Figure 5.** Combined radial distribution functions of  $[\text{PE}-(\text{AA})_{10}]_2$  for the centers of masses  $d(\text{PE-PE})$  and  $d(\text{PE-AA})$ .

populated conformations in the combined distribution functions. For example, PE-Glu shows multiple local maxima at  $d(\text{PE-PE})=1$  nm with  $d(\text{PE-AA})$  ranging from 1 to 3 nm. For aspartic acid, on the other hand, no such pattern of local maxima is visible; instead, the system has a broad peak at (3 nm, 2.5 nm). It should be noted that these combined distribution functions are averaged over about 50 ns, and show considerable evolution during this simulation period. A series of distribution functions for shorter time windows is given in Supporting Information for illustration.

This analysis cannot capture the full conformational space of the hybrid polymers due to incomplete statistical sampling convergence of the molecular dynamics simulation. However, the visible population of spatially extended conformations for early and late stages of the simulation (see Supporting Information) indicates that the structural sampling is most probably sufficient for a qualitative analysis.

The very distinct pattern for larger peptide segments observed in our simulations show that the actual chemistry of the amino acid type is decisive for the conformational distribution. Therefore, these hybrid polymers with a chain length of ten amino acids can be considered as peptide dominated structures, and the insertion of the synthetic polymer segments does not eliminate the individual structures from the peptide segment. The structure formation is clearly influenced by the polyethylene chains, but the peptide segment is long enough so that the individual chemistry of the amino acid side chains is able to contribute significantly to the secondary structure formation process.

### 3.2. Hybrid Polymer with Multiple Embedded PE Chain

A natural follow-up question is how much the structure of the peptide strand is changed if the peptide is “interrupted” multiple

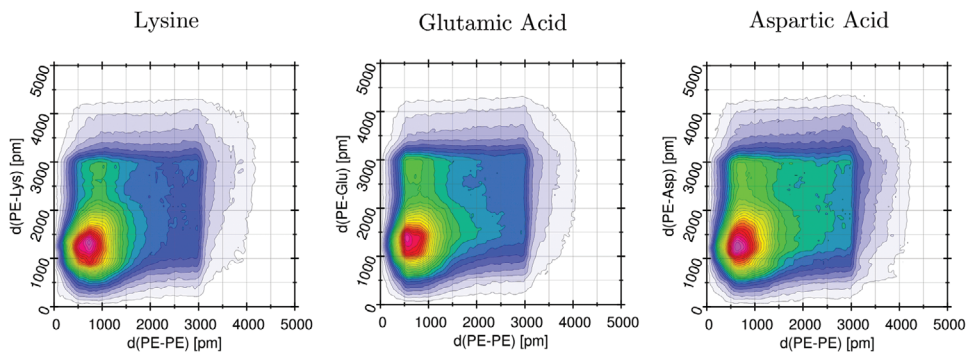


**Figure 6.** Combined radial distribution functions of  $[\text{PE}-(\text{AA})_3]_6$  for the centers of masses  $d(\text{PE}-\text{PE})$  and  $d(\text{PE}-\text{AA})$ .

times. We therefore switched from  $[\text{PE}-(\text{AA})_{10}]_2$  to  $[\text{PE}-(\text{AA})_3]_6$  molecules having a similar number of peptide residues but severely different peptide lengths. A preliminary hypothesis is that the hydrophobic properties of the PE chain overcome the peptide interaction and lead to a PE dominated structure. While this hypothesis is not supported by the Ramachandran plots in Table 2, we observe a visually quite strong difference in conformational pattern between  $[\text{PE}-(\text{AA})_{10}]_2$  and  $[\text{PE}-(\text{AA})_3]_6$ . Again, we utilize the combined distribution function  $g(d(\text{PE}-\text{AA}), d(\text{PE}-\text{PE}))$  shown in Figure 6. At first view, the patterns for  $[\text{PE}-(\text{AA})_3]_6$  look clearly distinct from the corresponding combined distribution function from the  $[\text{PE}-(\text{AA})_{10}]_2$  systems.

The combined distribution functions are independent of the amino acid type, which is at variance with the observations for the  $[\text{PE}-(\text{AA})_{10}]_2$  polymers. The favorable regions are also less scattered and show only a single maximum. Furthermore, the PE-PE distances are also more confined to lower distances compared to the PE-AA distance distribution, which suggests the peptide part to be more flexible for  $[\text{PE}-(\text{AA})_3]_6$  compared to  $[\text{PE}-(\text{AA})_{10}]_2$ . Besides the reduced length of the intermediate AA unit, this is caused by a lower amount of formed hydrogen bonds, shown by the average hydrogen bonds per residue over time in Figure 7. Due to the charged sidechains of the peptide segments the hydrogen bonds are considered to be only formed by the backbone. Overall, this indicates a structure dominated by the hydrophobic PE chains.

### 3.3. Influence of Total Chain Length

As a complementary question, we have investigated whether the conformational pattern of our hybrid polymers depends significantly on the number of repetitions of the elementary building block, that is, the number of monomer units  $m$  in  $[\text{PE}-(\text{AA})_n]_m$ . To this purpose, we have taken the  $[\text{PE}-(\text{AA})_3]_6$  systems (AA=Lys, Glu, Asp) and reduced the polymer index from  $m = 6$  to  $m = 2$ , which corresponds to the minimal meaningful version of this hybrid polymers.

The combined spatial distribution functions of the two characteristic effective distances  $d(\text{PE}-\text{AA})$  and  $d(\text{PE}-\text{PE})$  in the three systems is shown in Figure 8. The pattern shows an almost vanishing probability for PE-PE distances larger than 1 nm, and similarly low probabilities for PE-AA distances beyond 1.5 nm. No significant variations are observed upon exchange of the amino

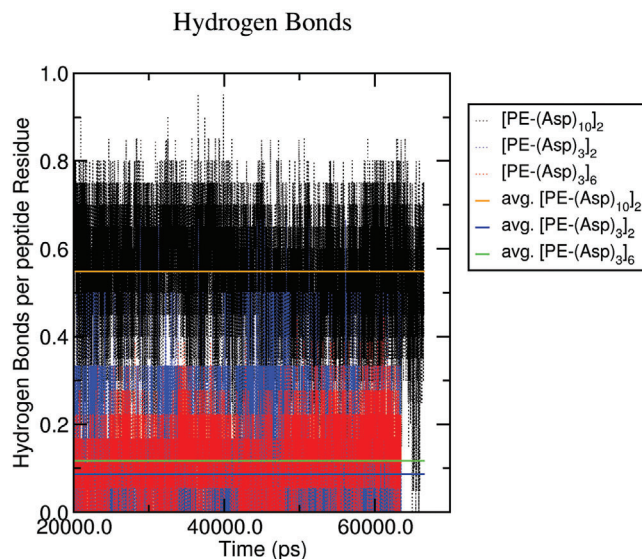


**Figure 7.** Time curve of the average number of backbone hydrogen bonds of one peptide residue to any other peptide for all  $[\text{PE}-(\text{Asp})_n]_m$ . This includes hydrogen bonds to peptides in the same unit, as well as hydrogen bonds to other peptide units, which are interrupted by a PE-chain. The number of hydrogen bonds is divided by the number of peptide residues to compare the systems, which is indicated by “per peptide residue.”

acid Lys/Glu/Asp. The considerable reduction of the distance distribution to the central peak near (0.5 nm, 1.0 nm) is even more apparent when comparing to the hybrid polymers of the same type but triple length (i.e.,  $[\text{PE}-(\text{AA})_3]_6$ ) in Figure 6. In the latter, the intermediate distances up to about 3 nm are visibly more frequent in the distribution. It should be noted that while the overall shape of the distribution function is still quite similar between  $m = 2$  and  $m = 6$ , the change in polymer length has a considerably larger effect than the variation of amino acid type.

Geometrically, the (PE-PE, PE-AA) peak distances around (0.5 nm, 1.0 nm) correspond to directly adjacent polymer strands. We have checked whether this spatial proximity is rather accidental or a direct consequence of hydrogen bonding, which is the most prominent structural driving force in peptides and proteins. The temporal evolution of the number of hydrogen bonds per amino acid during our trajectories is shown in Figure 7. The pattern for the hybrid polymers with short amino acid sequences

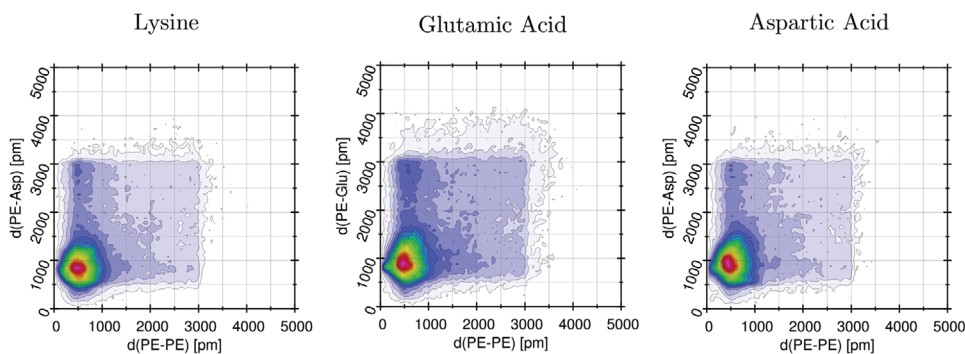


**Figure 8.** Combined radial distribution functions of  $[\text{PE}-(\text{AA})_3]_2$  for the centers of masses  $d(\text{PE}-\text{PE})$  and  $d(\text{PE}-\text{AA})$ .

(i.e.,  $n = 3$ , shown in red and blue) are very similar. This confirms the picture observed in the combined radial distribution functions (Figures 6 and 8). However, the polymers with longer amino acid chains ( $n = 10$ ) show a hydrogen bonding probability that is about five times higher. With an absolute value around 0.6, this probability is already close to the expected limit for a regular peptide of 0.8–0.9.

These findings illustrate that while the  $[\text{PE}-(\text{AA})_3]_6$  hybrid polymer has about the same total number of amino acids as  $[\text{PE}-(\text{AA})_{10}]_2$ , it behaves structurally much more like the minimalist  $[\text{PE}-(\text{AA})_3]_2$  polymer. On the other hand, the  $[\text{PE}-(\text{AA})_{10}]_2$  system is already similar to a regular peptide, despite the considerable perturbation from the polyethylene segment.

## 4. Conclusion

We have modeled the conformational space of a series of short peptides and their persistence upon perturbation of their peptide sequence by insertion of short, highly flexible polyethylene segments. Specifically, we have performed molecular dynamics simulations of  $[\text{PE}-(\text{AA})_{n,m}]$  (with  $\text{AA}=\text{Asp, Lys, Glu}$ ;  $n=\{3, 10\}$ ;  $m=\{2, 6\}$ ) in aqueous solution. The analysis of one- and 2D radial distribution functions and hydrogen bonds of these peptide/polymer segments shows that the secondary structure response to the inserted polyethylene chain is quite different for the three amino acid types. Upon frequent insertion (corresponding to a very short length  $n = 3$  of the peptide chain), we are unable to observe any meaningful secondary structure, independently of amino acid type and total length of the hybrid polymer.

Our results show that it is possible to locally suppress secondary structure motifs in peptides by means of inserting short synthetic polymer segments into the chain, and that this perturbation is restricted to about five to ten amino acids into the peptide.

## Supporting Information

Supporting Information is available from the Wiley Online Library or from the author.

## Acknowledgements

Funded by the Deutsche Forschungsgemeinschaft (DFG, German Research Foundation)—Project-ID 189853844—SFB/TRR 102.

Open access funding enabled and organized by Projekt DEAL.

## Conflict of Interest

The authors declare no conflict of interest.

## Data Availability Statement

The data that support the findings of this study are available from the corresponding author upon reasonable request.

## Keywords

hybrid bio/synthetic polymers, molecular dynamics simulations, peptide secondary structure

Received: November 10, 2022

Revised: February 6, 2023

Published online:

- [1] H. Elgabarty, M. Wolff, A. Glaubitz, D. Hinderberger, D. Sebastiani, *Phys. Chem. Chem. Phys.* **2013**, *15*, 16082.
- [2] C. Allolio, N. Salas-Illanes, Y. S. Desmukh, M. R. Hansen, D. Sebastiani, *J. Phys. Chem. B* **2013**, *117*, 9939.
- [3] T. Watermann, H. Elgabarty, D. Sebastiani, *Phys. Chem. Chem. Phys.* **2014**, *16*, 6146.
- [4] C. Schiffmann, D. Sebastiani, *Phys. Status Solidi B* **2012**, *249*, 368.
- [5] F. Hoffmann, J. Adler, B. Chandra, K. R. Mote, G. Bekçioğlu-Neff, D. Sebastiani, D. Huster, *J. Phys. Chem. Lett.* **2017**, *8*, 4740.
- [6] M. V. Vener, A. V. Odinokov, C. Wehmeyer, D. Sebastiani, *J. Chem. Phys.* **2015**, *142*, 215106.
- [7] G. Bekçioğlu-Neff, C. Allolio, Y. S. Desmukh, M. R. Hansen, D. Sebastiani, *ChemPhysChem* **2016**, *17*, 1166.
- [8] S. Pylaeva, M. Brehm, D. Sebastiani, *Sci. Rep.* **2018**, *8*, 13626.
- [9] F. Hoffmann, D.-W. Li, D. Sebastiani, R. Brüscheiler, *J. Phys. Chem. A* **2017**, *121*, 3071.
- [10] M. Brehm, M. Pulst, J. Kressler, D. Sebastiani, *J. Phys. Chem. B* **2019**, *123*, 3994.
- [11] R. Kiani, D. Sebastiani, P. Partovi-Azar, *ChemPhysChem* **2021**, *23*, 202100519.
- [12] P. Partovi-Azar, D. Sebastiani, *Batteries Supercaps* **2019**, *2*, 695.
- [13] S. Pylaeva, A. Böker, H. Elgabarty, W. Paul, D. Sebastiani, *ChemPhysChem* **2018**, *19*, 2931.
- [14] M. Cheon, I. Chang, C. K. Hall, *Proteins: Struct., Funct., Bioinf.* **2010**, *78*, 2950.
- [15] R. H. N. Kalaria, S. I. Harik, *J. Neurochem.* **1989**, *53*, 1083.

- [16] H. Y. Zoghbi, H. T. Orr, *Annu. Rev. Neurosci.* **2000**, *23*, 217.
- [17] C. M. Lill, C. Klein, *Nervenarzt* **2017**, *88*, 345.
- [18] C. Soto, *FEBS Lett.* **2001**, *498*, 204.
- [19] E. M. Bradbury, B. G. Carpenter, H. Goldman, *Biopolymers* **1968**, *6*, 837.
- [20] A. I. Arunkumar, T. K. Kumar, T. Sivaraman, C. Yu, *Int. J. Biol. Macromol.* **1997**, *21*, 299.
- [21] A. I. Arunkumar, T. K. S. Kumar, C. Yu, *Int. J. Biol. Macromol.* **1997**, *21*, 223.
- [22] C. Soto, *J. Mol. Med.* **1999**, *77*, 412.
- [23] C. Soto, *CNS Drugs* **1999**, *12*, 347.
- [24] E. Karran, B. De Strooper, *Nat. Rev. Drug Discov.* **2022**, *21*, 306.
- [25] G. B. Frisoni, D. Altomare, D. R. Thal, F. Ribaldi, R. van der Kant, R. Ossenkoppele, K. Blennow, J. Cummings, C. van Duijn, P. M. Nilsson, P. Y. Dietrich, P. Scheltens, B. Dubois, *Nat. Rev. Neurosci.* **2022**, *23*, 53.
- [26] M. Fändrich, C. M. Dobson, *EMBO J.* **2002**, *21*, 5682.
- [27] A. Lavasanifar, J. Samuel, G. S. Kwon, *Adv. Drug Delivery Rev.* **2002**, *54*, 169.
- [28] A. Lalatsa, A. G. Schätzlein, M. Mazza, T. B. H. Le, I. F. Uchegbu, *J. Controlled Release* **2012**, *161*, 523.
- [29] N. Liu, B. Li, C. Gong, Y. Liu, Y. Wang, G. Wu, *Colloids Surf., B* **2015**, *136*, 562.
- [30] J. Freudenberg, W. H. Binder, *Macromolecules* **2019**, *52*, 4534.
- [31] A. Carlsen, S. Lecommandoux, *Curr. Opin. Colloid Interface Sci.* **2009**, *14*, 329.
- [32] J. P. Chen, I. M. Chu, M. Y. Shiao, B. R. S. Hsu, S. H. Fu, *J. Ferment. Bioeng.* **1998**, *86*, 185.
- [33] M. Metzke, N. O'Connor, S. Maiti, E. Nelson, Z. Guan, *Angew. Chem., Int. Ed.* **2005**, *44*, 6529.
- [34] K. T. Al-Jamal, W. T. Al-Jamal, J. T. Wang, N. Rubio, J. Buddle, D. Gathercole, M. Zloh, K. Kostarelos, *ACS Nano* **2013**, *7*, 1905.
- [35] P. A. Taylor, A. Jayaraman, *Annu. Rev. Chem. Biomol. Eng.* **2020**, *11*, 257.
- [36] M. B. Canalp, W. H. Binder, *RSC Adv.* **2020**, *10*, 1287.
- [37] M. B. Canalp, A. Meister, W. H. Binder, *RSC Adv.* **2019**, *9*, 21707.
- [38] R. B. Merrifield, *J. Am. Chem. Soc.* **1963**, *85*, 2149.
- [39] C. Ho Wong, S. C. Zimmerman, *Chem. Commun.* **2013**, *49*, 1679.
- [40] C. Bonduelle, *Polym. Chem.* **2018**, *9*, 1517.
- [41] H. Sun, A. Brik, *Acc. Chem. Res.* **2019**, *52*, 3361.
- [42] S. Mohan, O. S. Oluwafemi, N. Kalarikkal, S. Thomas, S. P. Songca, in *Recent Advances in Biopolymers* (Ed: F. K. Perveen), Intech Open, London **2015**, Ch. 3.
- [43] V. Siracusa, I. Blanco, S. Romani, U. Tylewicz, P. Rocculi, M. Dalla Rosa, *J. Appl. Polym. Sci.* **2012**, *125*, S2.
- [44] A. Panáček, L. Kvítek, R. Pucek, M. Kolář, R. Večeřová, N. Pizúrová, V. K. Sharma, T. Nevěčná, R. Zbořil, *J. Phys. Chem. B* **2006**, *110*, 16248.
- [45] M. U. Sankar, S. Aigal, S. M. Maliyekkal, A. Chaudhary, Anshup, A. A. Kumar, K. Chaudhari, T. Pradeep, *Proc. Natl. Acad. Sci. U. S. A.* **2013**, *110*, 8459.
- [46] R. Rebelo, M. Fernandes, R. Figueiro, *Proc. Eng.* **2017**, *200*, 236.
- [47] G. Fuks, R. M. Talom, F. Gauffre, *Chem. Soc. Rev.* **2011**, *40*, 2475.
- [48] K. E. Gebhardt, S. Ahn, G. Venkatachalam, D. A. Savin, *J. Colloid Interface Sci.* **2008**, *317*, 70.
- [49] M. Morell, J. Puiggalí, *Polymers* **2013**, *5*, 188.
- [50] S. Matsumura, A. R. Hlil, C. Lepiller, J. Gaudet, D. Guay, Z. Shi, S. Holdcroft, A. S. Hay, *J. Polym. Sci. Part A Polym. Chem.* **2008**, *46*, 7207.
- [51] S. M. Kelly, T. J. Jess, N. C. Price, *Biochim. Biophys. Acta - Proteins Proteomics* **2005**, *1751*, 119.
- [52] J. Kong, S. Yu, *Acta Biochim. Biophys. Sin.* **2007**, *39*, 549.
- [53] W. K. Surewicz, H. H. Mantsch, D. Chapman, *Biochemistry* **1993**, *32*, 389.
- [54] A. Yaron, E. Katchalski, A. Berger, G. D. Fasman, H. A. Sober, *Biopolymers* **1971**, *10*, 1107.
- [55] M. Rinaudo, A. Domard, *J. Am. Chem. Soc.* **1976**, *98*, 6360.
- [56] G. Bussi, *Mol. Phys.* **2014**, *112*, 379.
- [57] L. Wang, R. Friesner, B. Berne, *J. Phys. Chem. B.* **2011**, *115*, 9431.
- [58] M. Bonomi, D. Branduardi, G. Bussi, C. Camilloni, D. Provasi, P. Raiteri, D. Donadio, F. Marinelli, F. Pietrucci, R. A. Broglia, M. Parrinello, *Comput. Phys. Commun.* **2009**, *180*, 1961.
- [59] G. A. Tribello, M. Bonomi, D. Branduardi, C. Camilloni, G. Bussi, *Comput. Phys. Commun.* **2014**, *185*, 604.
- [60] H. J. C. Berendsen, D. van der Spoel, R. van Drunen, *Comput. Phys. Commun.* **1995**, *91*, 43.
- [61] D. Van Der Spoel, E. Lindahl, B. Hess, G. Groenhof, A. E. Mark, H. J. Berendsen, *J. Comput. Chem.* **2005**, *26*, 1701.
- [62] N. Foloppe, A. D. MacKerell, *J. Comput. Chem.* **2000**, *21*, 86.
- [63] A. D. MacKerell, D. Bashford, M. Bellott, R. L. Dunbrack, J. D. Evanseck, M. J. Field, S. Fischer, J. Gao, H. Guo, S. Ha, D. Joseph-McCarthy, L. Kuchnir, K. Kuczera, F. T. Lau, C. Mattos, S. Michnick, T. Ngo, D. T. Nguyen, B. Prodhom, W. E. Reiher, B. Roux, M. Schlenkrich, J. C. Smith, R. Stote, J. Straub, M. Watanabe, J. Wiórkiewicz-Kuczera, D. Yin, M. Karplus, *J. Phys. Chem. B* **1998**, *102*, 3586.
- [64] B. Hess, *J. Chem. Theory Comput.* **2008**, *4*, 116.
- [65] W. Humphrey, A. Dalke, K. Schulten, *J. Mol. Graph.* **1996**, *14*, 33.
- [66] M. Brehm, B. Kirchner, *J. Chem. Inf. Model.* **2011**, *51*, 2007.
- [67] M. Brehm, M. Thomas, S. Gehrke, B. Kirchner, *J. Chem. Phys.* **2020**, *152*, 164105.